THE JOURNAL OF PHYSICAL CHEMISTRY B

Article

pubs.acs.org/JPCB

The Size of the Internal Loop in DNA Hairpins Influences Their Targeting with Partially Complementary Strands

Iztok Prislan, Hui-Ting Lee, Cynthia Lee, and Luis A. Marky*

Department of Pharmaceutical Sciences, University of Nebraska Medical Center, 986025 Nebraska Medical Center, Omaha, Nebraska 68198-6025, United States

ABSTRACT: Targeting of noncanonical DNA structures, such as hairpin loops, may have significant diagnostic and therapeutic potential. Oligonucleotides can be used for binding to mRNA, forming a DNA/RNA hybrid duplex that inhibits translation. This kind of modulation of gene expression is called the antisense approach. In order to determine the best strategy to target a common structural motif in mRNA, we have designed a set of stem-loop DNA molecules with sequence: d(GCGC**T**$_n$GTAAT_5GTTAC**T**$_n$GCGC), where n = 1, 3, or 5, "T_5" is an end loop of five thymines. We used a combination of calorimetric and spectroscopy techniques to determine the thermodynamics for the reaction of a set of hairpins containing internal loops with their respective partially complementary strands. Our aim was to determine if internal- and end-loops are promising regions for targeting with their corresponding complementary strands. Indeed, all targeting reactions were accompanied by negative changes in free energy, indicating that reactions proceed spontaneously. Further investigation showed that these negative free energy terms result from a net balance of unfavorable entropy and favorable enthalpy contributions. In particular, unfolding of hairpins and duplexes is accompanied by positive changes in heat capacity, which may be a result of exposure of hydrophobic groups to the solvent. This study provides a new method for the targeting of mRNA in order to control gene expression.

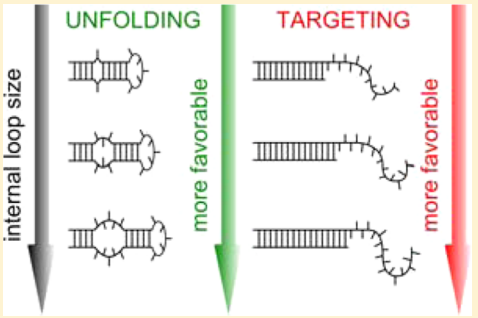

INTRODUCTION

It is now well established that DNA can adopt other conformations than the double helix first predicted by Watson and Crick.[1] Among these noncanonical DNA structures are stem-loop motifs that are involved in several biological functions.[2−5] Hence, targeted modulation of their properties have significant diagnostic and therapeutic potential. Besides a variety of compounds, such as the natural product Clerocidin,[6] nucleic acid oligonucleotides (ODNs) can also be used to target noncanonical DNA structures and RNA molecules. This latter approach is very selective since ODNs offer single-base specificity.[7] Chemically modified ODN's, which show higher resistance to nucleases, are also used[8−10] due to their availability, resistance to degradation in serum and low cytotoxic effect; however, unaltered DNA still remains a primary choice. There are several reported strategies wherein ODNs have been applied as modulators of gene expression. Since 1978, when Zamecnik and Stephenson used short synthetic oligonuceotides to modulate gene expression for the first time,[11] the antisense strategy has been studied extensively.[12−16] This approach predicts that binding of an ODN to mRNA yields a DNA/RNA duplex that sterically hinders the translation machinery or induces the cleavage of mRNA by RNase H.[17] The success of the strategy depends on several factors such as in vitro stability, membrane passage of ODNs, most critically on the sequence, structure and energetics of the ODNs. Poorly planned ODN sequences may target a very stable region in mRNA which does not permit the ODN to hybridize, thus strongly inhibiting its antisense activity.[18] The unfolding of mRNA tertiary and secondary structure requires energy, which is provided by formation of an ODN/RNA complex. The energy needed for unfolding the target region should be as low as possible, and the energy released from binding the ODN to mRNA should be as high as possible for antisense drugs to achieve maximum effect. This means that along with identifying and avoiding stable mRNA regions, special emphasis should be placed on the stability of the antisense ODN/RNA complex.[19] On the basis of this rationale, the loops of mRNA appear perfect candidates for targeting reactions since their unpaired bases are able to form additional base-pair stacks in the duplex products. The energy released from these interactions is able to overcome the energy needed to unfold the intramolecular structure of either the target or reactant.[20] The energy needed to unfold DNA/DNA, RNA/RNA and RNA/DNA duplexes is often predicted by nearest-neighbor thermodynamic parameters (N−N).[21−27] Comparison of DNA/DNA N−N[21−23] to DNA/RNA N−N[24−27] shows a high degree of similarity between the two duplexes. Therefore, it is suitable to mimic the targeting of RNA with DNA by using DNA instead of RNA as a target.

Our laboratory has a long record of using carefully planned sequences of DNA oligonucleotides to mimic RNA structures. We have examined the thermodynamic properties of several single stranded DNA complexes, including three-way junctions,

Received: October 7, 2014
Revised: December 4, 2014
Published: December 8, 2014

   dx.doi.org/10.1021/jp510131c | J. Phys. Chem. B 2015, 119, 96−104

Scheme 1. Investigated Targeting Reactions, Sequences, and Designations of Oligonucleotides

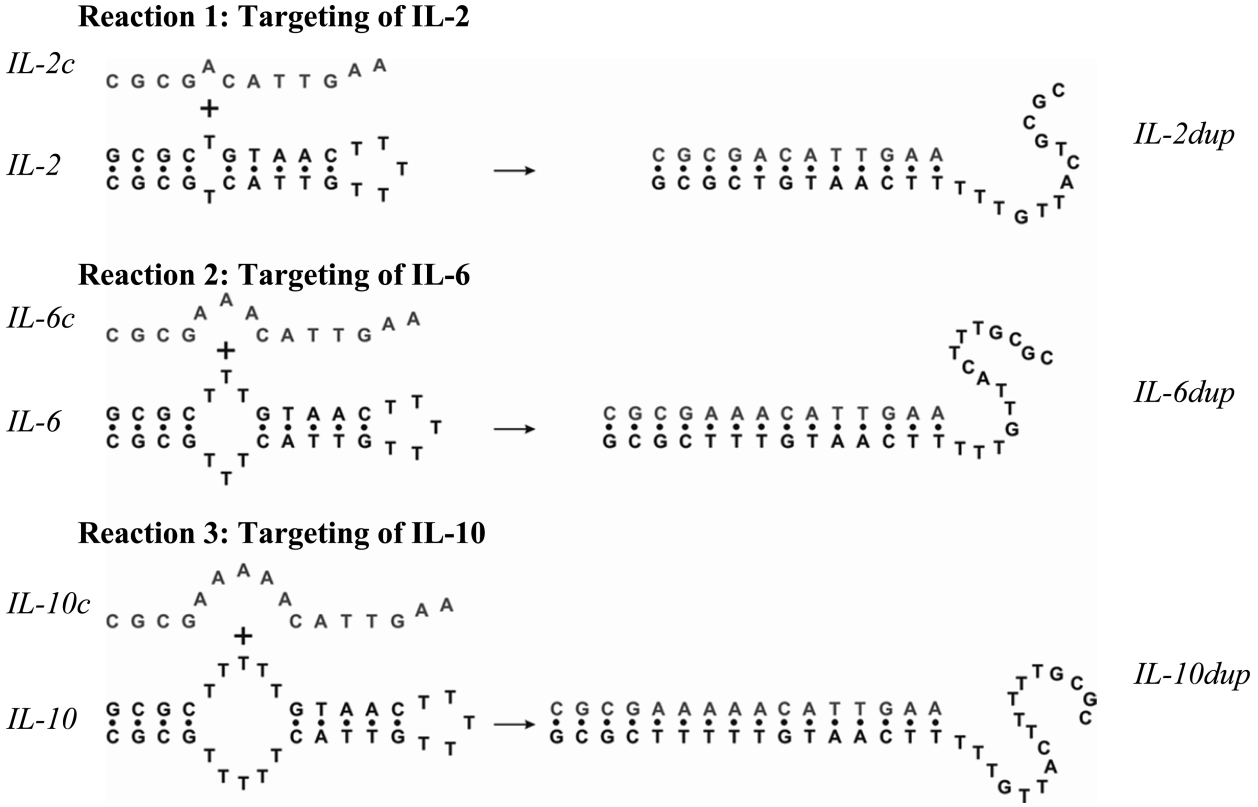

hairpins, and pseudoknots.[28−33] Subsequently, we targeted intramolecular DNA complexes with their complementary strands, and showed that single strands are able to disrupt the intramolecular complex and form stable duplex products.[20] In the current study, we focused on finding the best strategy to target hairpins in mRNA by varying the number of thymines in the internal loop of these motifs. To this end, we used a combination of isothermal titration (ITC) and differential scanning (DSC) calorimetry to determine thermodynamic profiles for the reaction of hairpins containing internal loops with their partially complementary strands. The results show that all reactions yielded favorable free energies in enthalpy driven processes. In these reactions, the single strand is able to invade and disrupt the hairpin to form a duplex product. Notably, the reaction free energies can be made more favorable by increasing the number of targeted bases within the loops.

MATERIALS AND METHODS

Materials. The oligonucleotides (ODNs) and their designations (Scheme 1): d(GCGCTGTAACT$_5$GTTACTGCGC), **IL-2**; d(GCGCT$_3$GTAACT$_5$GTTACT$_3$GCGC), **IL-6**; d(GCGCT$_5$GTAACT$_5$GTTACT$_5$GCGC), **IL-10**; d(AAGTTACAGCGC), **IL-2c**; d(AAGTTACA$_3$GCGC), **IL-6c**; d(AAGTTACA$_5$GCGC), **IL-10c** were synthesized by the Core Synthetic Facility of the Eppley Research Institute at UNMC, HPLC purified, and desalted by column chromatography using G-10 Sephadex exclusion chromatography. The concentrations in buffer solutions were determined spectrophotometrically at 25 °C using procedures reported previously.[28] Molar extinction coefficients for the single strands were estimated from the nearest-neighbor data of Cantor et al.[34] The results are listed as follows, in mM^{-1} cm^{-1} units: 221.9 (**IL-2**), 254.3 (**IL-6**), 286.7 (**IL-10**), 120.3 (**IL-2c**), 144.3 (**IL-6c**) and 168.3 (**IL-10c**). The extinction coefficients of 1:1 mixture of the ODN and complementary strands of Scheme 1 were calculated in the same way and the results are as follows, in mM^{-1} cm^{-1} units: 342.2 (**IL-2dup**), 398.6 (**IL-6dup**) and 455 (**IL-10dup**). Inorganic salts from Sigma were reagent grade, and used without further purification. Typical measurements were made in a buffer solution containing of 10 mM sodium phosphate, 0.1 M NaCl at pH 7.0. All oligonucleotide solutions were prepared by dissolving the dry and desalted ODNs in buffer, and then heating the solution to 90 °C for 5 min and cooling to room temperature over a period of 25 min.

Isothermal Titration Calorimetry (ITC). Buffer solution containing DNA hairpin was added stepwise to a buffer solution containing the complementary strand, and the reaction heat was measured by using the *i*TC$_{200}$ titration calorimeter from GE Healthcare, Microcal (Piscataway, NJ). A 40 μL syringe was used to inject the titrant (DNA hairpin); mixing was achieved by stirring this syringe at 1000 rpm; the temperature was kept constant at 20 °C. The complementary strand in the reaction cell ($C_{\text{IL-2c}}$ = 80 μM, $C_{\text{IL-6c}}$ = 80 μM, $C_{\text{IL-10c}}$ = 32 μM) was titrated by 6 injections of 0.6−1.8 μL of titrant ($C_{\text{IL-2}}$ = 80 μM, $C_{\text{IL-6}}$ = 80 μM, $C_{\text{IL-10}}$ = 40 μM). The enthalpy changes accompanying targeting reactions, ΔH_{ITC}, were obtained from the area under the measured peaks, corrected for the dilution heat of the titrant, and normalized by the moles of titrant added.[35] Results from six injections were collected and averaged yielding H_{ITC} for each targeting reaction.

To measure heat capacity effects, ΔC_p, we titrated each complementary strand at different temperatures (10−40 °C). The ΔC_p effects are obtained from the slopes of the ΔH_{ITC} versus temperature plots, where $\Delta H_{\text{ITC},T}$ is the reaction enthalpy at a given temperature T. All experiments were

dx.doi.org/10.1021/jp510131c | J. Phys. Chem. B 2015, 119, 96−104

Scheme 2. Cartoon of the Targeting Reaction Investigated by ITC and DSC: (a) Formation of Duplex Product When the Complementary Strand Is Targeted with a Hairpin or Vice Versa; (b) Example of a Hess Cycle[a]

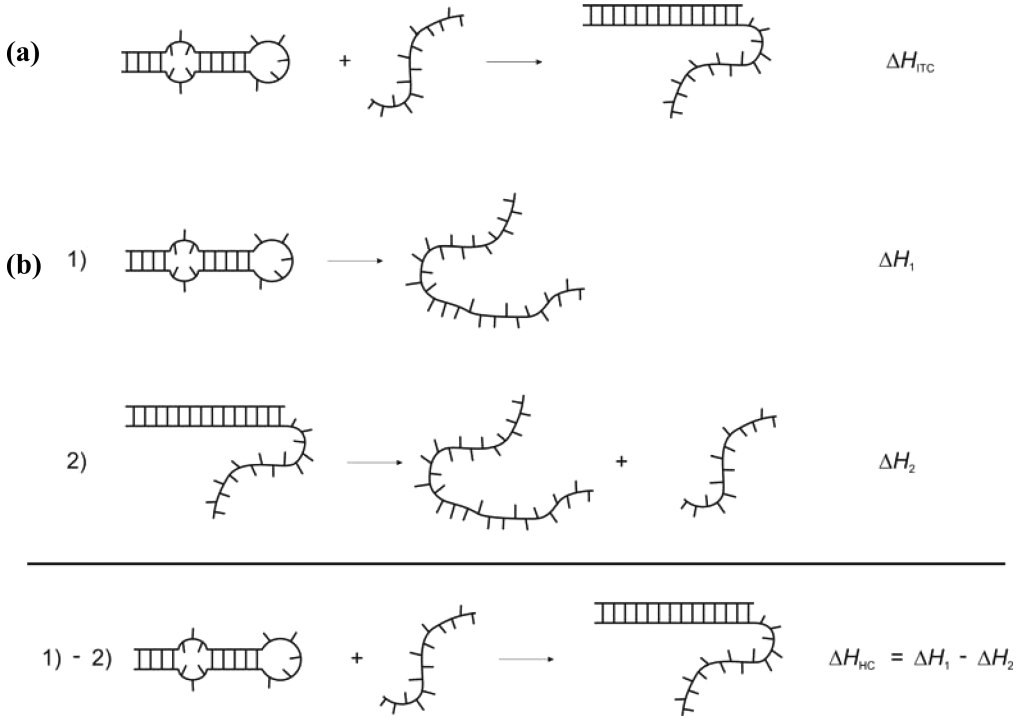

[a]Subtracting the DSC unfolding enthalpy of products from reactants yields the ITC targeting reaction which can be compared to the reaction shown in part a.

carried out in 10 mM sodium phosphate buffer at pH 7.0 and 0.1 M NaCl.

UV Melting Experiments. Absorbance versus temperature profiles of DNA samples were measured at 260 nm with the Aviv 14DS UV−vis spectrophotometer (Lakewood, NJ), which is equipped with a thermoelectric temperature controller. Changes in absorbance were monitored between 10 and 95 °C at a heating rate of 0.6 °C/min. Shape analysis of the melting curves and using standard procedures yielded transition temperatures (T_Ms) and van't Hoff enthalpies.[36] The transition molecularity for the unfolding of a hairpin or duplex was obtained by monitoring T_M as a function of strand concentration. Intramolecular hairpins show a T_M independent of strand concentration, whereas the T_M values of the bimolecular duplexes depend on strand concentration.[33] These T_M-dependences were used to estimate T_M values of duplex products at the concentrations used in the DSC experiments, and of the duplexes formed in the ITC titrations.

Differential Scanning Calorimetry (DSC). The VP-DSC differential scanning calorimeter from GE Healthcare, Microcal (Piscataway, NJ) was used to measure the heat associated with thermally induced unfolding of oligonucleotides (products and reagents of investigated targeting reactions). All scans were performed in the temperature range of 1−95 °C, using a heating rate of 0.75 °C/min. Analysis of the resulting thermograms yielded T_M values, and standard thermodynamic profiles, ΔH_{cal}, ΔS_{cal} and ΔG°_T. These parameters are obtained using the following relationships:[33] $\Delta H_{cal} = \int \Delta C_p(T)\, dT$ and $\Delta S_{cal} = \int \Delta C^a_p(T)/T\, dT$, where $\Delta C^a_p(T)$ represents the anomalous heat capacity during the transition. The Gibbs free energy at any temperature, ΔG°_T, is calculated with the Gibbs equation: $\Delta G^\circ_T = \Delta H_{cal} - T\Delta S_{cal}$. Alternatively, ΔG°_T can be calculated using the equation $\Delta G^\circ_T = \Delta H_{cal}(1 - T/T_M)$ for intramolecular transitions. DSC curves were recorded at several NaCl concentrations of 0, 0.1 M, and 0.2 M to determine indirectly whether unfolding of oligonucleotides is accompanied by changes in heat capacity (ΔC_p). ΔC_p values upon unfolding of products and reactants (Scheme 1) were calculated from the ΔH_{cal} versus T_M plots.[37] These ΔC_p effects allow us to estimate folding/unfolding enthalpies at any temperature using the standard thermodynamic relationship: $\Delta H(T_2) = \Delta H(T_M) - \Delta C_p(T_M - T_2)$.

Overall Experimental Approach. To better understand the targeting reactions under investigation (Scheme 1), the thermodynamic data obtained from ITC experiments were compared to the data obtained from DSC. First ITC was used to measure directly the enthalpy of reacting particular DNA structures with their complementary strands (ΔH_{ITC}). In the next step DSC was used to follow the unfolding of reactants and products of a given targeting reaction. DSC experiments were carried out at different salt concentrations to estimate the change in heat capacity upon unfolding of reactants and products. Kirchhoff's law was used to obtain the unfolding enthalpies at the temperature of each ITC experiment (20 °C), which according to the Hess's law of constant heat summation (see Scheme 2) can be used to calculate the enthalpy of each targeting reaction (ΔH_{HC_20}) and compare it to ITC data. Furthermore, we performed UV melting experiments of each duplex as a function of strand concentrations to establish the optimum temperature ranges for formation of a 100% duplex, where ITC experiments can be performed.

dx.doi.org/10.1021/jp510131c | J. Phys. Chem. B 2015, 119, 96−104

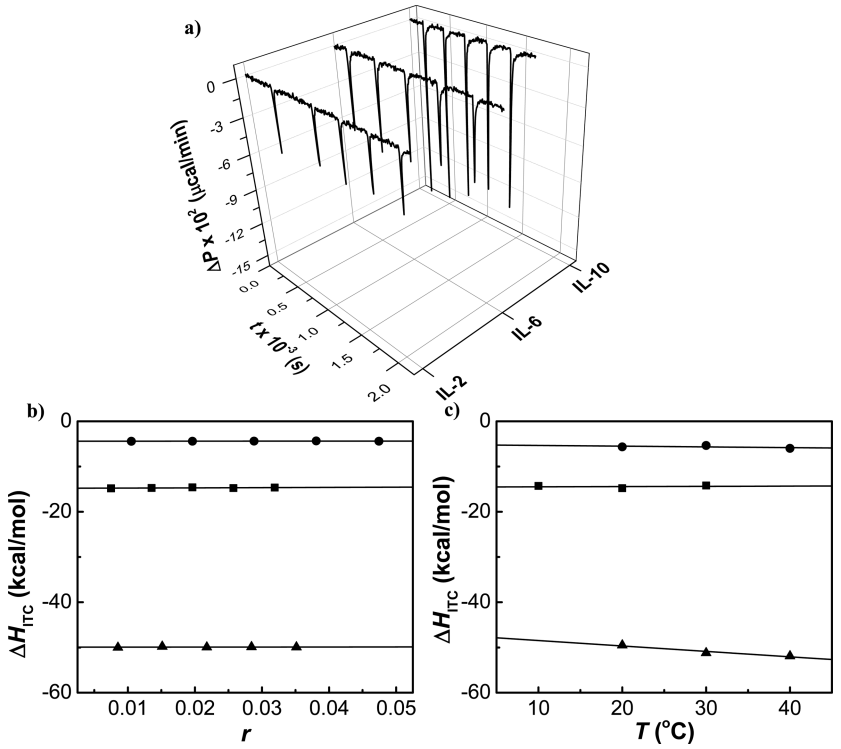

Figure 1. ITC titrations of partially complementary strands with hairpins in 10 mM sodium phosphate buffer, 0.1 M NaCl, at pH 7.0. (a) Raw data for titrations under unsaturated condition and (b) the resulting ΔH_{ITC} values for formation of **IL-2** duplex (●), **IL-6** duplex (■), and **IL-10** duplex (▲) (c) Temperature dependence of ΔH_{ITC} values for formation of **IL-2** duplex (●), **IL-6** duplex (■), and **IL-10** duplex (▲).

RESULTS AND DISCUSSION

All targeting reactions yielded exothermic heats. We have used ITC to measure the heats for each targeting reaction of Scheme 1. Figure 1 shows the ITC titrations at 20 °C for the reaction of each hairpin with their respective complementary strand. The hairpin solution was placed in the syringe and the reaction cell was filled with its complementary strand solution. The average of six injections yielded exothermic heats that correspond to ΔH_{ITC} values of −4.4, −14.9 and −49.9 kcal/mol for the formation of **IL-2dup**, **IL-6dup** and **IL-10dup**, respectively. These values result from the net balance of endothermic and exothermic contributions. Endothermic contributions result from disruption of both hairpin base-pair stacks and base−base stacking of the complementary strands, which are completely overridden by exothermic contributions due to the formation of base-pair stacks of the duplex product.

We have also carried out ITC experiments at different temperatures. The results of Figure 1 show similar ΔH_{ITC} values, indicating the absence of heat capacity effect i.e, ΔC_p = 0.

We used DNA nearest neighbor parameters to predict the unfolding enthalpy of the hairpin reactants and duplex products. Complementary base-pair stacking contributions were calculated according to methods described previously.[38,39] The contributions of the loop thymines were also taken into account by only including the base pairs adjacent to stems as T·T mismatches.[40] We obtained enthalpies of 81, 79 and 78 kcal/mol for the formation of **IL-2**, **IL-6**, and **IL-10**, respectively, and 91, 107 and 123 kcal/mol for the formation of **IL-2dup**, **IL-6dup**, and **IL-10-dup**, respectively. Using Hess cycles, we predict ΔH values of −10, −27 and −45 kcal/mol for the formation of **IL-2dup**, **IL-6dup**, and **IL-10-dup**, respectively (Scheme 2). Comparison of the predicted values with the experimentally measured ΔH_{ITC} values shows a discrepancy of 8 kcal/mol on average. We suggest that the reasons for this discrepancy are as follows: (1) heat capacity effects were not included in the N−N enthalpies, (2) the actual percentage of duplex formation, which might be lower than 100%, and (3) the contributions from single strand base−base stacking of partially complementary strands. These contributions will be discussed in later sections.

The products **IL-6dup** and **IL-10dup** unfolded in monophasic transition, but the UV melting curve for **IL-2** shows two transitions. The first one with T_M = 51 °C corresponds to unfolding of the duplex and the second one with T_M = 68 °C corresponds to the unfolding of the hairpin. All three curves show a hyperchromic effect, which increases with increasing the size of the duplex from 13% (**IL-2dup**) to 19% (**IL-10dup**). The T_M values of the transition of each duplex follow the order 50 °C (**IL-2**) < 54.8 °C (**IL-10**) < 56.6 °C (**IL-6**) and correspond to more base-pair stacking. In contrast to hairpin unfolding, the unfolding of each duplex at different concentrations yields different T_M values for the transitions (Figure 2, right panel). This result raises a question: is the formation of duplexes complete at the concentration and temperature used in ITC experiments? We used the T_M dependences on strand concentration to determine the actual T_M of a given duplex at the concentration used in the ITC experiments.

UV and DSC Unfolding. Typical UV melting curves are shown in the left panels of Figure 2. The sigmoidal shapes of UV melting curves suggest that all three hairpins unfold cooperatively, indicating a monophasic nature of unfolding. The helix−coil transitions are accompanied by a hyperchromic effect which ranges from 11% (**IL-6**) to 19% (**IL-2**). Increasing the internal loop or lowering the percentage of GC base pairs in

dx.doi.org/10.1021/jp510131c | J. Phys. Chem. B 2015, 119, 96−104

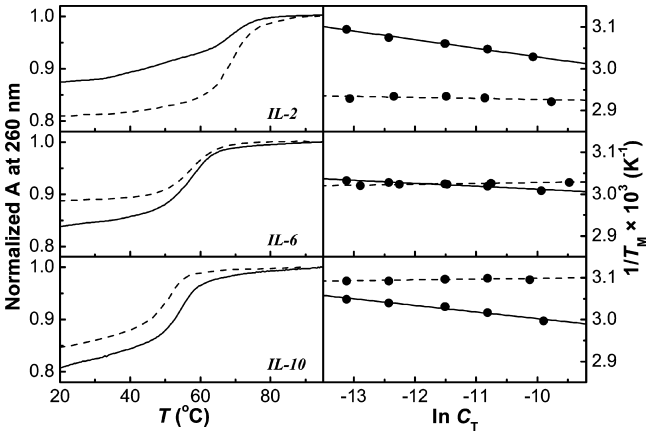

Figure 2. Left panels show normalized UV melting curves at 260 nm for the duplexes (full line) and hairpins (dashed line). Right panels show the changes in T_M when the concentration of duplex (full line) or hairpin (dashed line) is increased. All experiments were carried out in 10 mM sodium phosphate buffer at pH 7.0 and 0.1 M NaCl.

hairpins results in drop of the T_M of the transition; 68.2 °C (**IL-2**) > 57.6 °C (**IL-6**) > 50.4 °C (**IL-10**). Even 10-fold increase in oligonucleotide strand concentration fails to change the T_M values of the transitions (Figure 2 − right panels), suggesting intramolecular unfolding.[36]

Figure 3 shows the DSC unfolding curves of the reactants and products of each reaction, and Table 1 has the standard thermodynamic profiles for the unfolding of each reactant and product. **IL-2**, **IL-6**, **IL-6dup**, **IL-10**, and **IL-10dup** show clear monophasic transitions whereas **IL-2dup** shows two transitions.

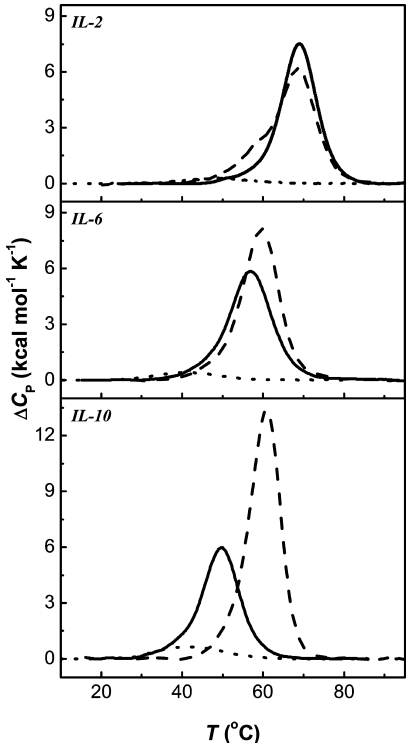

Figure 3. DSC curves of hairpins (full lines), duplexes (dashed lines) and complementary strands (dotted lines). All experiments were carried out in 10 mM sodium phosphate buffer at pH 7.0 and 0.1 M NaCl.

The first and smaller transition occurs at T_M of 57.5 °C and the second one occurs at T_M of 69.9 °C. Comparison of these values with the ones obtained from the UV melting curve shows that the T_M of the first peak changes by 6 °C and T_M of the second peak is about the same. The duplex concentration in the DSC experiment is about 20 times higher than the one in the UV melt, which suggests that the T_M of the structure that is unfolding first is concentration dependent. This indicates that the first transition corresponds to the unfolding of a bimolecular duplex while the second transition corresponds to unfolding of an intramolecular hairpin. The magnitude of the DSC peak that corresponds to the unfolding of **IL-2dup** appears be too low to represent unfolding of a duplex because this peak results from two processes—unfolding of duplex and formation of hairpins. Since energy is needed to break base-pair stacking and energy is released upon formation of new bonds, the magnitude of the first peak is much lower than expected. The reason for having two transitions in DSC thermogram is the lower stability of **IL-2dup** relative to **IL-2**. If we compare the T_M values of the other duplexes and hairpins (Table 1), we can see that in the case of **IL-6** the T_M of duplex is approximately the same as T_M of hairpin and in the case of **IL-10** the T_M of duplex is higher than the T_M of hairpin.

The product duplexes yielded enthalpies of 87.8 (**IL-2dup**), 110.2 (**IL-6dup**), and 139.6 kcal/mol (**IL-10dup**). These enthalpies are in good agreement with those estimated from nearest-neighbor parameters, 91 (**IL-2dup**), 107 (**IL-6dup**), and 123 kcal/mol (**IL-10dup**) without the heat contributions from the dangling ends. The increase in stability and enthalpy of unfolding is due to the increase in the number of base-pair stacking interactions.

All three partially complementary strands showed a transition (Figure 3) with unfolding heats of 5, 8.5, and 13 kcal/mol (Table 1), and DSC T_Ms of 49, 40, and 41 °C. This indicates that there are base−base stacking interactions present in the solution of these complementary strands. Before binding to the hairpins these interactions need to be disrupted and energy is needed for this process to take place. As a result the favorable enthalpy of binding, observed during the ITC experiments, will be lowered.

Heat Capacity Contributions. We did not find heat capacity effects between the initial and final states of the DSC curves for the unfolding of all products and reactants (Figure 3), i.e., $\Delta C_p = 0$. The sensitivity of the VP-DSC calorimeter does not allow measurement of heat capacity effects that are within the experimental noise of the DSC baselines (40 cal/°C-mol base pair) but they may still be present. To determine whether heat capacity effects accompany the unfolding of oligonucleotides, an indirect approach was used. DSC experiments were conducted at different NaCl concentrations (Figure 4, parts a and c) and plots of ΔH_{cal} as a function of T_M were constructed (Figure 4, parts b and d). These plots yielded straight lines with positive slopes, which correspond to positive ΔC_p values for the unfolding of hairpins (Table 1) of 970 (**IL-2**), 630 (**IL-6**), and 310 cal/°C (**IL-10**) and also positive ΔC_p values for the unfolding of duplexes of 1000 (**IL-2dup**), 650 (**IL-6dup**), and 290 cal/°C (**IL-10dup**). This result shows that the unfolding of each hairpin/duplex is accompanied by an exposure of hydrophobic groups to the solvent. Nonpolar groups push away water molecules and thus bring order to the hydration shell relative to bulk water.[41] For instance, unfolding of **IL-10** results in the lowest change in heat capacity suggesting that the thymine bases of the internal loop are exposed to the

dx.doi.org/10.1021/jp510131c | J. Phys. Chem. B 2015, 119, 96−104

Table 1. Thermodynamic Profiles for Reactants and Products of Each Targeting Reaction[a]

	T_M (°C)	ΔH_{cal} (kcal/mol)	$\Delta G°_{20}$ (kcal/mol)	$T\Delta S_{cal}$ (kcal/mol)	ΔC_p (cal/°C mol)	ΔH_{corr} (kcal/mol)	$\Delta G°_{corr}$ (kcal/mol)	$T\Delta S_{cal}$ (kcal/mol)
				Reaction 1				
IL-2	69.1 ± 0.5	86 ± 4	12.4 ± 0.9	74 ± 4	970 ± 60	39 ± 9	8.8 ± 1.4	30 ± 10
IL-2dup	57.0 ± 0.5	88 ± 4	10.1 ± 0.5	77 ± 4	1000 ± 60	49 ± 9	9.4 ± 1.2	40 ± 10
IL-2c	49.0 ± 0.5	5.0 ± 0.3	/	/	/	/	/	/
				Reaction 2				
IL-6	57.0 ± 0.5	82 ± 4	9.2 ± 0.5	73 ± 4	630 ± 30	59 ± 6	7.8 ± 0.9	51 ± 7
IL-6dup	59.2 ± 0.5	110 ± 6	13.0 ± 0.7	97 ± 5	650 ± 40	85 ± 9	11.4 ± 1.3	73 ± 10
IL-6c	40.0 ± 0.5	8.5 ± 0.4	/	/	/	/	/	/
				Reaction 3				
IL-10	49.8 ± 0.5	76 ± 4	7.1 ± 0.4	69 ± 3	310 ± 70	67 ± 9	6.6 ± 0.7	60 ± 10
IL-10dup	60.9 ± 0.5	140 ± 7	17.0 ± 0.9	112 ± 6	290 ± 80	130 ± 13	16.3 ± 1.4	111 ± 14
IL-10c	41.0 ± 0.5	13.0 ± 0.7	/	/	/	/	/	/

[a]All experiments were carried out in 10 mM sodium phosphate buffer at pH 7.0 and 0.1 M NaCl. The experimental unfolding thermodynamic profiles were corrected for heat capacity effects. Experimental errors are shown in parentheses: T_M (±0.5 °C), ΔH_{cal} (±5%), $\Delta G°_{20}$ (±7%) and $T\Delta S_{cal}$ (±5%).

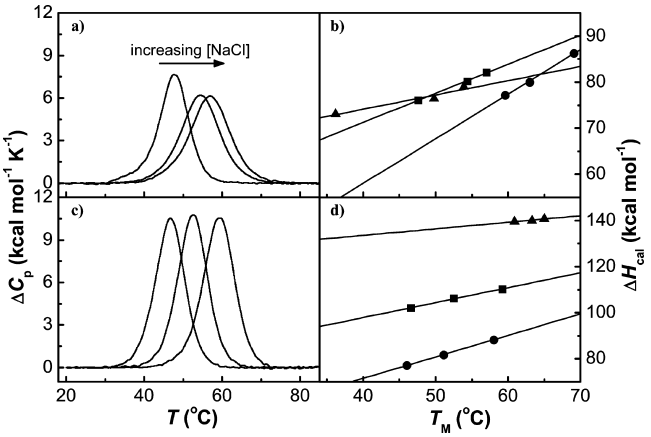

Figure 4. DSC thermograms as a function of salt concentration used to obtain heat capacity effects. (a) Typical DSC curves of **IL-6** at different salt concentrations. (b) Heat capacity plots of **IL-2** (●), **IL-6** (■), and **IL-10** (▲) (c) Typical DSC curves of **IL-6dup** at different salt concentrations. (d) Heat capacity plots of **IL-2dup** (●), **IL-6dup** (■), and **IL-10dup** (▲). All experiments were carried out in 10 mM sodium phosphate buffer, at pH 7 and at total Na^+ concentrations of 16, 56, and 116 mM.

solvent in a similar way as in random coil state. In other words, our results show that the thymine bases are not orientated toward each other (inside the internal loop) but outward–toward the solvent. On the other hand the highest change in heat capacity is upon unfolding of **IL-2**, which suggest that the helical state of **IL-2** is the most hydrophilic one, this is consistent with a fully paired stem.

One notable observation is that similar heat capacity effects accompany the unfolding of the hairpins and of the duplexes. According to the Hess cycle, this finding means that a heat capacity effect should not be present for each targeting reaction, since ΔC_p of hairpin and duplex cancel each other out. The results of ITC experiments indicate that ΔH_{ITC} values are independent of temperature thus confirming our Hess cycle prediction of a $\Delta C_p = 0$ for each targeting reaction or duplex formation.

Targeting Reactions Using Hess Cycles. According to the Hess law the enthalpies of targeting reaction can be calculated by subtracting the unfolding enthalpy of the duplex from that of the reactant (Scheme 2), yielding enthalpy values, ΔH_{HC}, of −1.5, −27.9, and −63.2 kcal/mol. When comparing these values to ΔH_{ITC} obtained from ITC titrations, we calculated discrepancies of 3.9 (**IL-2**), 13 (**IL-6**), and 13.3 kcal/mol (**IL-10**) (Table 2). The unfolding enthalpies of duplex and reactant obtained from DSC correspond to T_M values and Kirchhoff's law has to be used to extrapolate them to the temperature of the ITC experiment. After correcting unfolding enthalpies of hairpins and duplexes for the heat capacity effects (Figure 4), the Hess cycle yielded enthalpy values, ΔH_{HC_20}, of −10.1, −25.9, and −60.5 kcal/mol (Table 2). The ΔH_{HC_20} differ from the ΔH_{ITC} (in absolute values) by 5.6, 11, and 10.6 kcal/mol, respectively. Although including the heat capacity effect in our calculation accounted for some discrepancy between the data obtained from the Hess cycle and from the

Table 2. Thermodynamic Profiles for the Targeting Reactions[a]

	DSC			ITC			
	ΔH_{HC_20} (kcal/mol)	ΔH_{HC_corr} (kcal/mol)	ΔG_{HC_corr} (kcal/mol)	ΔH_{ITC} (kcal/mol)	ΔC_p (cal/°C mol)	$\Delta H_{ITC\_corr.}$ (kcal/mol)	$\Delta G°_{ITC\_20}$ (kcal/mol)
reaction 1: targeting of **IL-2**	−2 ± 4	−10 ± 9	−1 ± 2	−4.4 ± 0.2	−20 ± 30	−9.4 ± 0.5	−1 ± 2
reaction 2: targeting of **IL-6**	−28 ± 5	−26 ± 8	−4 ± 2	−14.9 ± 0.7	5 ± 30	−23 ± 1	−3 ± 2
reaction 3: targeting of **IL-10**	−63 ± 6	−61 ± 11	−10 ± 2	−50 ± 2	−120 ± 30	−63 ± 3	−10 ± 3

[a]All experiments were carried out in 10 mM sodium phosphate buffer at pH 7.0 and 0.1 M NaCl. Experimental error for ΔH_{ITC} was estimated at ±5%.

dx.doi.org/10.1021/jp510131c | J. Phys. Chem. B 2015, 119, 96–104

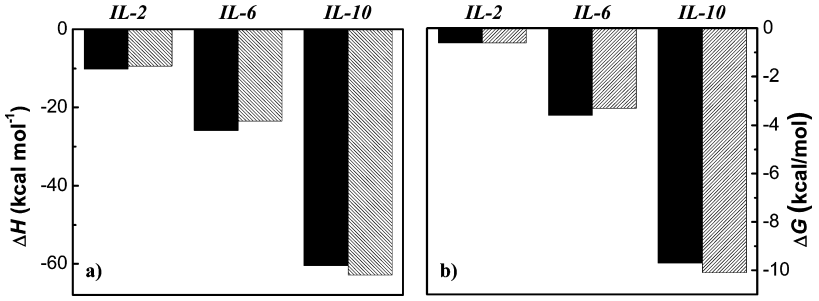

Figure 5. Enthalpy and free energy for targeting reactions in 10 mM sodium phosphate buffer at pH 7 and 0.1 M NaCl. (a) Comparison between enthalpy values calculated from Hess cycle and corrected for heat capacity effect (solid building blocks) and enthalpy values obtained from ITC data and corrected for complementary single strand stacking interactions (hatched building blocks) (b) Comparison between free energy values calculated from Hess cycle and corrected for heat capacity effect (solid building blocks) and free energy values obtained from ITC data and corrected for complementary single strand stacking interactions (hatched building blocks).

ITC titrations, the values are still apart by an average of 9 kcal/mol. In order to explain and resolve discrepancies in enthalpies obtained from ITC and DSC, we have to take into account the temperatures at which the targeting and unfolding reactions are followed and the behavior of complementary strands. ITC reactions reflect endothermic contributions from disruption of base-pair stacking of the hairpins and base−base stacking in the complementary strands and exothermic contributions due to the formation of base-pair stacks in the duplex product. In the DSC Hess cycles, we take into consideration the enthalpy contributions for the unfolding of hairpins and the formation of product duplex, but due to higher temperatures of unfolding of the duplexes and the absence of free complementary strands, the Hess cycle does not include potential base−base stacking interactions. DSC melting curves of each complementary single strand showed that base−base stacking interactions are present, and these could be measured. If we use the measurements to correct the enthalpies obtained from ITC experiments, the resulting enthalpy values, ΔH_{ITC_corr}, are −9.4, −23.4, and −62.9 kcal/mol for the formation of **IL-2dup**, **IL-6dup**, and **IL-10dup**, respectively. If we compare these values to the ones obtained from Hess cycle, we can see that by taking into account both the heat capacity effect and single strand base−base stacking interactions, the average discrepancy reduces to about 2 kcal/mol. (Table 2, Figure 5)

Thermodynamic Profiles for Targeting of Hairpins. To determine the free energy, ΔG°_{ITC}, for each targeting reaction, we use the following relationship, reported earlier: $\Delta G^\circ_{ITC} = \Delta G^\circ_{HC}$ ($\Delta H^\circ_{ITC}/\Delta H^\circ_{HC}$), where ΔG°_{HC} is calculated from the DSC data in a similar manner as the ΔH_{HC} terms, using the following relationship for each of the reactants: $\Delta G^\circ_{HC} = \Delta H_{cal} - T\Delta S_{cal} + \Delta C_p[(T - T_M) - T \ln(T/T_M)]$, where T is the temperature of ITC titrations. Thermodynamic profiles for all targeting reactions are listed in Table 2 and shown as building blocks in Figure 5. All of the enthalpies of duplex formation are exothermic and thus favorable. According to the Hess cycle, the favorable enthalpies for formation of duplexes increase from −10.1 to −60.5 kcal/mol as the number of thymines of the internal loops rises from 2 to 10. This result is primarily due to the increase in the number of base-pairs that can be formed. ITC experiments also yield favorable enthalpy effects upon formation of duplexes that increase with the size of the duplex from −9.4 (**IL-2dup**) to −62.9 kcal/mol (**IL-10dup**). After including heat capacity effects and single strand base−base stacking interactions, the enthalpies for formation of duplexes obtained from the Hess cycle and ITC experiments are almost the same (Figure 5). In terms of the overall free energy contribution at 20 °C, ΔG°_{20}, we obtained favorable ΔG°_{20} terms (Table 2), indicating that all targeting reactions proceed spontaneously. The favorable Gibbs free energies calculated from the Hess cycle increase from −0.6 to −9.4 kcal/mol as the loop size is increased from 2 to 10 thymines. The values obtained from the Hess cycle and those obtained from ITC experiments show very good agreement (Table 2, Figure 5)

In summary, our results show that increasing the number of targeted bases in the internal loops of hairpins results in more favorable targeting reactions with complementary strands, which should be taken into consideration when the antisense approach is used to modulate gene expression. These targeting reactions are effectively enthalpy driven due to release of heat from product formation.

CONCLUSIONS

The antisense strategy uses short synthetic oligonuceotides to modulate gene expression. Designing oligonucleotides to target loops of mRNA appears to be a promising approach because the unpaired bases are able to form additional base-pair stacks in the duplex products. Formation of additional base-pair stacks releases energy, needed to unfold the intramolecular structure of either the target or reactant. We have mimicked the targeting of RNA by using DNA instead of RNA as a target, which is known to be a good model system. Three stem-loop DNA molecules with increasing number of thymines in the internal loop and an end loop of five thymines were designed and targeted with partially complementary DNA single strands. Thermodynamic profiles for these targeting reactions were obtained by combining experimental data obtained from ITC, UV-spectroscopy and DSC. ITC was used to measure reaction enthalpies directly, whereas DSC unfolding enthalpies were used to create Hess cycle to calculate reaction enthalpies indirectly. The values obtained from the Hess cycles and those obtained from ITC experiments are in good agreement, and revealed that interaction of DNA intramolecular complexes with complementary strands is favorable and enthalpy driven. The favorable enthalpy of targeting reactions results from stronger exothermic contribution of additional base-pair stacks formed in the duplex products relative to endothermic contributions from the disruption of both base-pair stacks of the hairpins and base−base stacking interactions of the single strands. This occurs due to unpaired bases in the internal loops forming additional base pairs and base-pair stacks upon reaction with complementary sequences, thus providing the energy

dx.doi.org/10.1021/jp510131c | J. Phys. Chem. B 2015, 119, 96−104

necessary for disruption of DNA intramolecular structures. In general increasing the length of single strands with complementary sequences and/or the size of internal loop of DNA intramolecular structures will result in higher free energy term and higher stability of the duplex products. This study demonstrates the importance of studying thermodynamics of nucleic acid targeting reactions to develop optimal ODN sequences to modulate gene expression.

AUTHOR INFORMATION

Corresponding Author

*(L.A.M.) Telephone: (402) 559-4628. E-mail: lmarky@unmc.edu.

Notes

The authors declare no competing financial interest.

ACKNOWLEDGMENTS

This work was supported by Grants MCB-0616005 and MCB-1122029 from the National Science Foundation, and a Shared Instrumentation Grant 1S10RR027205 from the National Institutes of Health. Partial financial support (to I.P.) from the Slovenian Research Agency (P1 0201) is greatly appreciated.

REFERENCES

(1) Delmonte, C. S.; Mann, L. R. B. Variety in DNA Secondary Structure. *Curr. Sci.* **2003**, *85*, 1564−1570.

(2) Posey, J. E.; Malgorzata, J. P.; Sinden, R. R.; Roth, D. B. Target DNA Structure Plays a Critical Role in RAG Transposition. *PLoS Biol.* **2006**, *4*, 1934−1946.

(3) Bikard, D.; Loot, C.; Baharoglu, Z.; Mazel, D. Folded DNA in Action: Hairpin Formation and Biological Functions in Prokaryotes. *Microbiol. Mol. Biol. Rev.* **2010**, *74*, 570−588.

(4) Zhu, L.; Chou, S.-H.; Reid, B. R. A Single G-to-C Change Causes Human Centromere TGGAA Repeats to Fold back into Hairpins. *Proc. Natl. Acad. Sci. U.S.A.* **1996**, *93*, 12159−12164.

(5) Smith, G. R. Meeting DNA palindromes head-to-head. *Genes Dev.* **2008**, *22*, 2612−2620.

(6) Nadai, M.; Palu, G.; Palumbo, M.; Richter, S. N. Differential Targeting of Unpaired Bases within Duplex DNA by the Natural Compound Clerocidin: A Valuable Tool to Dissect DNA Secondary Structure. *PLoS One* **2012**, *7*, 1−12.

(7) Crooke, S. T. Molecular Mechanisms of Antisense Drugs. *Biochim. Biophys. Acta—Gene Struct. Expr.* **1999**, *1489*, 31−43.

(8) Freier, S. M.; Altmann, K.-H. The ups and downs of Nucleic Acid Duplex Stability: Structure-Stability Studies on Chemically-Modified DNA:RNA Duplexes. *Nucleic Acid Res.* **1997**, *25*, 4429−4443.

(9) Lesnik, E. A.; Freier, S. M. What Affects the Effect of 2′-alkoxy Modifications? 1. Stabilization Effect of 2′-methoxy Substitutions in Uniformly Modified DNA Oligonucleotides. *Biochemistry* **1998**, *37*, 6991−6997.

(10) Yoo, B. H.; Bochkareva, E.; Bochkarev, A.; Mou, T.-C.; Gray, D. M. 2′-O-methyl-Modified Phosphorothioate Antisense Oligonucleotides have Reduced Non-Specific Effects in Vitro. *Nucleic Acid Res.* **2004**, *32*, 2008−2016.

(11) Stephenson, M. L.; Zamecnik, P. C. Inhibition of Rous sarcoma viral RNA translation by a specific oligodexyribonucleotide. *Proc. Natl. Acad. Sci. U.S.A.* **1978**, *75*, 285−288.

(12) Gewirtz, A. M.; Sikol, D. L.; Ratajczak, M. Z. Nucleic Acid Therapeutics: State of the Art and Future Prospects. *Blood* **1998**, *92*, 712−736.

(13) Crooke, S. T. *Antisense drug technology: principles, strategies, and applications*; CRC Press, Taylor and Francis Group: Boca Raton, FL, 2008.

(14) Dias, N.; Stein, C. A. Antisense Oligonucleotides: Basic Concepts and Mechanisms. *Mol. Cancer Ther* **2002**, *1*, 347−355.

(15) Clark, R. E. Antisense therapeutics in chronic myeloid leukaemia: the promise, the progress and the problems. *Leukemia* **2000**, *17*, 347−355.

(16) Bennett, C. F.; Swayze, E. E. RNA targeting therapeutics: molecular mechanisms of antisense oligonucleotides as a therapeutic platform. *Annu. Rev. Pharmacol. Toxicol.* **2010**, *50*, 259−293.

(17) Hélène, C. Control of Oncogene Expression by Antisense Nucleic Acids. *Eur. J. Cancer* **1994**, *30A*, 1721−1726.

(18) Sugimoto, N.; Yasumatsu, I. A new Concept for the Design of Antisense Oligonucleotides Based on Nucleic Acid Thermostability. *Curr. Med. Chem.* **2001**, *1*, 95−112.

(19) Lee, H.-T.; Olsen, C. M.; Waters, L.; Sukup, H.; Marky, L. A. Thermodynamic Contributions of the Reactions of DNA Intramolecular Structures with their Complementary Strands. *Biochimie* **2008**, *90*, 1052−1063.

(20) Breslauer, K. J.; Frank, R.; Blöcker, H.; Marky, L. A. Predicting DNA Duplex Stability from the Base Sequence. *Proc. Natl. Acad. Sci. U.S.A.* **1986**, *83*, 3746−3750.

(21) Sugimoto, N.; Nakano, S.; Yoneyama, M.; Honda, K. Improved Thermodynamic Parameters and Helix Initiation Factor to Predict Stability of DNA Duplexes. *Nucleic Acids Res.* **1996**, *24*, 4501−4505.

(22) Gray, M. Derivation of Nearest-Neighbor Properties from Data on Nucleic Acid Oligomers. I. Simple Sets of Independent Sequences and the Influence of Absent Nearest Neighbors. *Biopolymers* **1997**, *42*, 783−793.

(23) Gray, M. Derivation of Nearest-Neighbor Properties from Data on Nucleic Acid Oligomers. II. Thermodynamic Parameters of DNA·RNA Hybrids and DNA Duplexes. *Biopolymers* **1997**, *42*, 795−810.

(24) Xia, T.; SantaLucia, J., Jr.; Burkard, M. E.; Kierzek, R.; Schroeder, S. J.; Jiao, X.; Cox, C.; Turner, D. H. Thermodynamic Parameters for an Expanded Nearest-Neighbor Model for Formation of RNA Duplexes with Watson-Crick Base Pairs. *Biochemistry* **1998**, *37*, 14719−14735.

(25) Sugimoto, N.; Nakano, S.; Katoh, M.; Matsumura, A.; Nakamuta, H.; Ohmichi, T.; Yoneyama, M.; Sasaki, M. Thermodynamic Parameters to Predict Stability of RNA/DNA Hybrid Duplexes. *Biochemistry* **1995**, *34*, 11211−11216.

(26) Lu, Z. J.; Turner, D. H.; Mathews, D. H. A Set of Nearest Neighbor Parameters for Predicting the Enthalpy Change of RNA Secondary Structure Formation. *Nucleic Acids Res.* **2006**, *34*, 4912−4924.

(27) Marky, L. A.; Blumenfeld, K. S.; Kozlowski, S.; Breslauer, K. J. Salt-Dependent Conformational Transitions in the Self-Complementary Deoxydodecanucleotide d(CGCAATTCGCG): Evidence for Hairpin Formation. *Biopolymers* **1983**, *22*, 1247−1257.

(28) Marky, L. A.; Kallenbach, N. R.; McDonough, K. A.; Seeman, N. C.; Breslauer, K. J. The Melting Behavior of a DNA Junction Structure: a Calorimetric and Spectroscopic Study. *Biopolymers* **1987**, *26*, 1621−1634.

(29) Rentzeperis, D.; Shikiya, R.; Maiti, S.; Ho, J.; Marky, L. A. Folding of Intramolecular DNA Hairpin Loops: Enthalpy-Entropy Compensations and Hydration Contributions. *J. Phys. Chem. B* **2002**, *106*, 9945−9950.

(30) Prislan, I.; Lee, H.-T.; Lee, C.; Marky, L. A. *ACS Symposium Series; Frontiers in Nucleic Acids* **2011**, *1082*, 93−110.

(31) Soto, A. M.; Loo, J.; Marky, L. A. Energetic Contributions for the Formation of TAT/TAT, TAT/CGC(+), and CGC(+)/CGC(+) Base Triplet Stacks. *J. Am. Chem. Soc.* **2002**, *124*, 14355−14363.

(32) Soto, A. M.; Rentzeperis, D.; Shikiya, R.; Alonso, M.; Marky, L. A. DNA Intramolecular Triplexes Containing dT –> dU Substitutions: Unfolding Energetics and Ligand Binding. *Biochemistry* **2006**, *45*, 3051−3059.

(33) Cantor, C. R.; Schimmel, P. R. *Biophysical Chemistry Part III: the Behavior of Biological Macromolecules*; W. H. Freeman and Company: New York, 1980.

(34) Wiseman, T.; Williston, S.; Brandts, J. F.; Lin, L.-N. Rapid Measurement of Binding Constants and Heats of Binding Using a New Titration Calorimeter. *Anal. Biochem.* **1989**, *179*, 131−137.

(35) Marky, L. A.; Breslauer, K. J. Calculating Thermodynamic Data for Transitions of any Molecularity from Equilibrium Melting Curves. *Biopolymers* **1987**, *26*, 1601−1620.
(36) Shikiya, R.; Marky, L. A. Calorimetric Unfolding of Intramolecular Triplexes: Length Dependence and Incorporation of Single AT → TA substitutions in the duplex domain. *J. Phys. Chem. B* **2005**, *109*, 18177−18183.
(37) SantaLucia, J., Jr.; Hicks, D. The Thermodynamics of DNA Structural Motifs. *Annu. Rev. Biophys. Biomol. Struct.* **2004**, *33*, 415−440.
(38) Zuker, M. Mfold web server for nucleic acid folding and hybridization prediction. *Nucleic Acids Res.* **2003**, *31*, 3406−3415, URL http://mfold.rna.albany.edu/.
(39) Peyret, N.; Seneviratne, A.; Allawi, H. T.; SantaLucia, J., Jr. Nearest-Neighbor Thermodynamics and NMR of DNA Sequences with Internal A-A, C-C, G-G, and T-T Mismatches. *Biochemistry* **1999**, *38*, 3468−3477.
(40) Madan, B.; Sharp, K. A. Hydration Heat Capacity of Nucleic Acid Constituents Determined from the Random Network Model. *Biophys. J.* **2001**, *81*, 1881−1887.
(41) Cullis, P. M.; Wolfenden, R. Affinities of Nucleic Acid Bases for Solvent Water. *Biochemistry* **1981**, *20*, 3024−3028.